Colloids and Surfaces B: Biointerfaces 167 (2018) 397–406

Contents lists available at ScienceDirect

Colloids and Surfaces B: Biointerfaces

journal homepage: www.elsevier.com/locate/colsurfb

Characterization of hybrid microparticles/Montmorillonite composite with raspberry-like morphology for Atorvastatin controlled release

Perla García-Guzmán[a], Luis Medina-Torres[b], Fausto Calderas[c], María Josefa Bernad-Bernad[b], Jesús Gracia-Mora[b], Baltasar Mena[d], Octavio Manero[a,*]

[a] Instituto de Investigaciones en Materiales, Universidad Nacional Autónoma de México (UNAM), Circuito Exterior S/N, Coyoacán, Cd. Universitaria C.P.04510, Ciudad de México, Mexico
[b] Facultad de Química, Universidad Nacional Autónoma de México (UNAM), Circuito Exterior S/N, Coyoacán, Cd. Universitaria C.P.04510, Ciudad de México, Mexico
[c] Facultad de Estudios Superiores (FES) Zaragoza, Universidad Nacional Autónoma de México (UNAM), Campus II Batalla 5 de mayo s/n esquina Fuerte de Loreto, Col. Ejército de Oriente, Iztapalapa C.P. 09230, Ciudad de México, Mexico
[d] Instituto de Ingeniería, Universidad Nacional Autónoma de México (UNAM), Circuito Exterior S/N, Coyoacán, Cd. Universitaria C.P.04510, Ciudad de México, Mexico

ARTICLE INFO

Article history:
Received 30 December 2017
Received in revised form 22 March 2018
Accepted 4 April 2018
Available online 9 April 2018

Keywords:
Rheology
Montmorillonite
Hybrid microparticles
Gelatin
Atorvastatin
Drug delivery

ABSTRACT

In this work, we prepared a novel composite based on hybrid gelatin carriers and montmorillonite clay (MMT) to analyze its viability as controlled drug delivery system. The objective of this research involves the characterization of composites formed by structured lipid-gelatin micro-particles (MP) and MMT clay. This analysis included the evaluation of the composite according to its rheological properties, morphology (SEM), particle size, XRD, FT-IR, and *in vitro* drug release. The effect of pH in the properties of the composite is evaluated. A novel *raspberry-like* or *armor* MP/MMT clay composite is reported, in which the pH has an important effect on the final structure of the composite for *ad-hoc* drug delivery systems. For pH values below the isoelectric point, we obtained defined morphologies with entrapment efficiencies up to 67%. The pH level controls the MP/MMT composite release mechanism, restringing drug release in the stomach-like environment. Intended for oral administration, these results evidence that the MP/MMT composite represents an attractive alternative for intestinal-colonic controlled drug delivery systems.

1. Introduction

Atorvastatin (AC) ([R-(R/, R/)]-2-(4-fluorophenyl)-b, d-dihydroxy-5-(1-methylethyl)-3-phenyl-4 [(phenylamino) carbonyl] – 1H-pyrrole-1-heptanoic acid) is widely prescribed as a cholesterol-lowering agent. It belongs to the second generation of statins as a synthetic reversible inhibitor of the microsomal enzyme 3-hydroxy-3-methyl-glutaryl-coenzyme A (HMG-CoA) reductase which catalyzes the rate-limiting step in cholesterol biosynthesis. AC is rapidly absorbed after oral administration, but possesses poor bioavailability (∼12%) attributed to instability in stomach acidic medium, crystalline properties, low aqueous solubility and high hepatic first-pass metabolism. Usually an administration of high doses and longtime therapies is necessary, although it is related to adverse effects particularly rhabdomyolysis, liver abnormalities and kidney failure may be present [1].

Several approaches considered the enhancement of oral bioavailability and water solubility of drugs, including micro and nano-carriers based on polymers, lipids, oils, proteins, polysaccharides, inorganic materials and so on. Various studies with Atorvastatin have reported enhanced oral bioavailability and efficacy, including nanoparticles of poly(lactic-co-glycolic acid) (PLGA) [2,3], chitosan [4], Eudragit [5] and poly(ε-caprolactone) [6] are include.

In the development of new drug carriers, each material provides distinct advantages. However, a strategy to use drug-carriers hybridization involves the design of a new delivery vehicle named lipid-polymer hybrid carrier, which combines the characteristics of polymeric nanoparticles and liposomes [7–11]. With these systems, some studies pointed out the improvement in drug loading capacity, solubility, bioavailability and sustained release to oral administration [10,12]. In addition, clays and polymer blends constitute novel hybrid drug delivery systems also known as

* Corresponding author.
E-mail address: manero@unam.mx (O. Manero).

https://doi.org/10.1016/j.colsurfb.2018.04.020
0927-7765/

polymer-clay composites. Clays have an important role in pharmaceutical formulations used as excipients and active agents. Clays may interact with drug molecules and other formulation components such as polymers. The addition of clays can improve polymer properties related to controlled-release systems, namely, swelling, erosion, biodegradation and dissolution. Various mechanisms are involved in the interaction between clays and polymers such as hydrogen-bonding, dipole–dipole interactions, covalent bonding and electrostatic interactions or cation exchange, depending on the polymer type and pH of the medium [13]. Polymer-clay composites are prepared by several methods, in particular: (1) intercalation of polymers from solution; (2) intercalation of polymers from melt, (3) *in situ* intercalative polymerization and (4) template synthesis methods [14].

Montmorillonite (MMT) has become prominent among other clays due to its abundance, environmentally friendliness and well-studied chemistry. MMT is a natural material with high internal surface area, high cation exchange capacity (CEC), high adsorption and swelling ability, low or null toxicity, good biocompatibility and it is a material "generally recognized as safe" (GRAS) by the FDA [15–17]. MMT is a layered hydrate aluminum silicate which belongs to the smectite group of phyllosilicates. The layer thickness of each platelet is in the order on 1 nm and the lateral dimension is approximately 200 nm. These platelets are composed of one Al-octahedral sheet (O) sandwiched between two Si-tetrahedral sheets (T). The triple sheet structure is stacked in layers bound together by van der Waals forces and is referred as 2:1 (T-O-T) layer configuration of tactoids. It possesses a net negative charged face (F) due to isomorphous ionic substitution in the T-O-T structure, compensated by interlayer hydrated cations potentially exchanged by cations and organic molecules. In addition, MMT possesses a pH-dependent charge in their edges (E), with reported isoelectric point (IEP) between 5.0 and 7.0. This allows face-to-face (F-F), edge-to-face (E-F) and edge-to-edge (E-E) interactions leading to formation of different particle associations like "*house-of-cards*" at pH < 7.0, which are responsible for interesting rheological properties such as its viscosity and viscoelastic response [13,18,19].

On the other hand, due to its negative permanent charge, MMT may be a safe candidate to prepare composites by electrostatic interactions with cationic polymers, like gelatin (GEL). GEL is a biopolymer derived from collagen with ample applications in pharmacy and medicines due to its biodegradability, biocompatibility in physiological environments, low-cost, readily available and low antigenicity. In addition, due to its gel-forming properties, GEL has been extensively studied with relation to the preparation of micro and nanocarriers, including nanoparticles for swelling controlled delivery of chloroquine phosphate [20] and insulin [21]. The inherent cationic property of GEL is due to lysine and arginine residues; [22] thus, GEL shows cationic behavior at pH values below the IEP via protonation of amine groups. GEL properties can be tuned easily by pH, ionic strength and temperature without any additional complex functionalization [23,24]. In the literature, several authors have reported the preparation of GEL/MMT composites for controlled drug delivery such as intercalation of pure GEL chains [13], hydrogel systems [25] and nanoparticles [26]. Nevertheless, it has been reported that the addition of MMT inside GEL carriers reduces the entrapment efficiency and drug loading capacity [17,26,27]. Hence, it is highly recommended to search for composites of various structures keeping high the drug entrapment efficiency and taking advantage of MMT controlled release properties with Atorvastatin (a low water-soluble drug). Since GEL is an amphoteric biopolymer, the interaction with MMT may depend on the pH of the medium for composite preparation and mechanism/rate release. The objective of this research was the preparation of a novel composite of hybrid microparticles (lipid-polymer) and MMT clay and to evaluate the effect of Gastrointestinal tract (GIT) pH conditions on Atorvastatin controlled release. In addition, measurements of particle size, zeta potential, infrared spectroscopy (FT-IR), X-ray powder diffraction (XRD), scanning electron microscopy (SEM) and rheological characterization may shed light into the structure-properties relationship of this composite.

2. Materials and methods

2.1. Materials

Gelatin (type B, gel strength ~225 g Bloom), Lecithin (L-α-Phosphatidylcholine from egg yolk, ~60% TLC), methylene blue, Atorvastatin calcium salt trihydrate (AC) and Montmorillonite clay (Na^+ MMT) NanoClay Nanomer® from Sigma-Aldrich were used as received. Materials included Glutaraldehyde (GA) grade I (25% solution in water) from Merck, regenerate cellulose dialysis bags (MWCS 12–14 kDa) from Spectra/Por, USA, ultrapure water of quality 18.2 MΩ cm at 25.0 ± 1 °C from distilled water with a Barnstead Nanopure diamond system. All buffer solutions were prepared according to the USP30-NF25 and all other reagents and solvents were analytical grade.

2.2. Preparation of lipid-polymer hybrid microparticles (MP)

The lipid-polymer hybrid microparticles (MP) were prepared by the previously reported two-step desolvation method [28,29], with slight modifications as per laboratory conditions. Briefly, GEL (200.0 mg) was dissolved in deionized water (10.0 mL) at 40.0 ± 1 °C. High molecular weight (HMW) GEL chains were precipitated by addition of acetone (10.0 mL) as desolvating agent. The supernatant was discarded and the precipitated HMW GEL was re-dissolved in deionized water (10.0 mL) at 40.0 ± 1 °C. The pH was adjusted to 3.0 ± 0.1 with HCl 0.2 M. AC (10.0 mg) and lecithin (100.0 mg) were dissolved in methanol (5.0 mL), the resulting AC/lecithin solution was added to the HMW GEL solution drop-wise under constant stirring at 750 rpm. Methanol was evaporated at room conditions for 12 h and acetone (10.0 mL) was added drop-wise under constant stirring to precipitate hybrid MP. Finally, an aqueous solution of Glutaraldehyde (2% v/v, 25 μL) was added as a cross-linking agent and stirred for 12 h at 750 rpm. The AC loaded MP were centrifuged at 14 000 rpm (Sorvall Biofuge Primo R) during 30 min at room temperature, the supernatant was discarded and the pellet was re-dispersed in deionized water two times. The MP dispersion was freeze-dried at −50.0 ± 1 °C and 0.024 mBar for 48 h (Labconco free zone triad).

2.3. Characterization of lipid-polymer hybrid microparticles (MP)

2.3.1. Entrapment efficiency (EE%)

Entrapment efficiency of AC was determined by mixing the MP dispersion (0.5 mL) with acetone (1.0 mL) and sonicated for 1 h (Cole-Parmer Ultrasonic) at room temperature with a high-frequency output of 42 kHz. The solution was centrifuged at 14 000 rpm for 30 min (Sorvall Biofuge Primo R); the supernatant was analyzed by UV–vis Spectrophotometric method with a S2000 spectrometer using a DT1000 deuterium light source, a SAD500 serial port interface (Ocean Optics, Inc.), with 10 mm path length quartz cuvette (Prolab). Measurements were performed in triplicate at room temperature and the data was presented in mean ± SD. The entrapment efficiency (Eq. (1)) was calculated as follows:

$$\text{Entrapment Efficiency}\,(\%) = \frac{\text{Amount of AC in microparticles}}{\text{Total amount of AC}} \qquad (1)$$

2.4. Preparation of microparticle/MMT clay composite (MP/MMT)

The MP/MMT composite was prepared by an exfoliation/adsorption from solution and evaporation method previously reported [30] with slight modifications. An amount of MMT clay (50.0 mg) was added to deionized water and adjusted to pH = 3.0 ± 0.1 (2.0 mL) with HCl 0.2 M and sonicated during 30 min (Cole-Parmer Ultrasonic) at room temperature with a high-frequency output of 42 kHz. A fresh MP dispersion (5.0 mL) adjusted to pH = 3.0 ± 0.1 was added dropwise to the MMT clay dispersion and stirred for 1 h at 750 rpm under room conditions. The MP/MMT composite dispersion was verted in a petri dish and air dried at 25.0 ± 1 °C for 12 h.

2.5. Cation exchange capacity (CEC) and surface area (S_{BET}) determination

The CEC determination of MMT clay was made according to the standard test method for methylene blue index of clay (ASTM C 837-81). An amount of clay (2.0 g) was placed in a beaker; deionized water (300.0 mL) was added and sufficient sulfuric acid to bring the pH within 2.5–3.8. After the adjusting the pH, a burette was filled with methylene blue solution (0.1 meq mL^{-1}) added (5.0 mL) to the slurry and stirred for 1–2 min. Finally, a drop of the slurry was placed on a filter paper. The methylene blue solution was added in increments of 1.0 mL under constant stirring, after each addition a drop was added on filter paper. The end point was indicated by the formation of a light blue halo around the drop [31]. The CEC (Eq. (2)) was calculated as follows:

$$CEC = \frac{E * V}{W} 100 \quad (2)$$

where, ***CEC*** is the cation exchange capacity in equivalents 100 g^{-1} of clay, ***E*** represents equivalents of methylene blue per milliliter, ***V*** represents the milliliters of methylene blue solution required for the titration and ***W*** is grams of dry clay.

Brunauer-Emmett-Teller (BET) surface area (S_{BET}) was obtained from N_2 adsorption-desorption isotherms at 77 K measured on a *Nova 2200e (QuantaChrome Instruments)* after degassing the sample under vacuum for 24 h at 120.0 ± 1 °C for MMT clay raw powder.

2.6. MP, MMT and MP/MMT clay composite characterization

2.6.1. Particle size and zeta potential (ξ)

The hydrodynamic diameter and polydispersity index (PDI) were determined by dynamic light scattering (DLS) using a Zetasizer Zen3600 (Malvern Instruments) at 25.0 ± 1 °C with 173° backscatter as angle of detection for MP, MMT and MP/MMT composite. MMT (10.0 mg mL^{-1}) was dispersed with magnetic stirring during 30 min, after that the dispersion was sonicated (Cole-Parmer Ultrasonic) with a high-frequency output of 42 kHz during 30 min at room temperature. All measurements were taken in triplicate and the data was presented in mean ± SD.

Zeta Potential (ξ) of MP, MMT and MP/MMT composite was evaluated by electrophoretic light scattering. The surface charge of MP and MMT was determined with the dispersion (100.0 μL) diluted to 1.5 mL with 10.0 mM NaCl solution adjusting the pH to values between 3.0 ± 0.1 and 8.0 ± 0.1, using HCl 0.2 M or NaOH 0.2 M. The NaCl solution compensated for the conductivity effect resulting from the addition of HCl or NaOH [32]. The Zeta potential of the final MP/MMT composite was evaluated in deionized water. All measurements were taken in triplicate at room temperature and the data was presented in mean ± SD.

2.6.2. Fourier-transform infrared (FT-IR) spectroscopy

The MP, MMT clay raw powder and MP/MMT composite were characterized by FT-IR. Transmission infrared spectra were recorded with a FTIR/FIR Spectrum 400 spectrophotometer (Perkin-Elmer). The infrared spectra of the samples were measured over a wavelength range of 4000–400 cm^{-1}.

2.6.3. XRD powder diffraction

X-ray powder diffraction (XRD) determinations on powdered MMT clay alone and MP/MMT clay composite, within the scattering angle range of 2θ = 2–70 at the rate of 0.01°s^{-1}. To evaluate the pH effect on the interaction, XRD patterns were recorded in the MP/MMT composite followed by adjusting the pH ± 0.1 to 1.6, 3.0, 5.0, 6.5 and 7.0, using HCl 0.2 M or NaOH 0.2 M. XRD and air dried at room conditions for 12 h. XRD patterns were analyze with software Match! 3®.

2.6.4. Shape and morphology by scanning electron microscopy (SEM)

The shape and surface morphology were determined by scanning electron microscopy (SEM) (JSM-35 CF, JEOL) with 20 kV. A drop of MP dispersion or MP/MMT composite was deposited, air-dried at room conditions and coated with gold to obtain a conducting surface. Finally, the sample was analyzed under vacuum. The pH effect on morphology was analyzed by SEM in MP/MMT composite prepared at different pH conditions (namely pH = 3.0 ± 0.1 and 7.0 ± 0.1).

2.7. Rheological characterization

Rheological measurements were performed in a stress-controlled model TA Instruments Discovery HR3® rheometer using a concentric cylinders geometry (21.96 mm outer diameter, 20.38 mm inner diameter, 59.90 mm height and 500 μm gap).

To analyze the pH effect on the rheological behavior, MP and MP/MMT composite were re-suspended in deionized water at 25.0 ± 1 °C (10 mg mL^{-1}), adjusting the pH ± 0.1 to 3.0, 4.8 and 7.0 using HCl 0.2 M or NaOH 0.2 M. Samples were characterized under steady-simple shear flow in the range from 1 to 100 s^{-1}, and under oscillatory flow in the linear viscoelastic regime, previously determined for each experimental conditions (γ < 50%) at 37.0 ± 1 °C. The angular frequencies ***(ω)*** of the tests ranged from 1 to 100 rad/s at 37.0 ± 1 °C (circulating water bath Cole Parmer Polystat and Peltier AR-G2). Both ***G′*** (elastic) and ***G″*** (viscous) moduli served to analyze the viscoelastic behavior of the samples. All data were analyzed by one-way analysis of variance (ANOVA) and a value of ($p < 0.05$) was considered statistically significant [33].

2.8. In vitro *drug release studies*

The drug release profile was measured by the dialysis bag method. An amount of MP or MP/MMT composite was loaded into a pre-swelled dialysis bag. The dialysis assembly was then suspended in release medium (100.0 mL) at 37.0 ± 1 °C in a closed beaker with constant magnetic stirring (250 rpm). The study was carried out using different media to simulate GIT pH conditions considering the effect of food intake on pH and the transit time [34]. For the study in the fasted-state (FAS) the dialysis bag was first soaked in a simulated gastric fluid (SGF), a hydrochloric acid buffer solution pH 1.6 ± 0.1 (FAS-SGF) and kept for 2 h. Then, it was transferred into simulated intestinal fluid (SIF) (100.0 mL) of phosphate buffer solution pH 6.5 ± 0.1 (FAS-SIF) and kept for 6 h. Finally, it was extracted and immersed in simulated colonic fluid (SCF) (100.0 mL), a phosphate buffer solution pH 7.0 ± 0.1 (FAS-SCF) for 40 h. For the fed-state (FED) an acetate buffer solution was used at of pH 5.0 ± 0.1 (FED-SGF), a phosphate buffer solution with pH

of 5.8 ± 0.1 (FED-SIF) and pH of 7.0 ± 0.1 (FED-SCF). At determined time intervals, a volume of the release medium was withdrawn and assayed by UV–vis spectrophotometric method. An equal amount of fresh medium, which was preheated to 37.0 ± 1 °C, was added for compensation after each sample drawing to maintain sink conditions. All the experiments were performed in triplicate and the data was presented in mean ± SD. A Spectrophotometric (UV) analysis of AC was carried out at wavelength of maximum absorbance (λ_{max}=243.07 nm). The analyze was performed in a S2000 spectrometer using a DT1000 deuterium light source, SAD500 serial port interface (Ocean Optics, Inc.) and 10 mm path length quartz cuvette (Prolab). Statistical comparisons were made using one-way analysis of variance (ANOVA). A value of $p < 0.05$ was considered statistically significant. Data processing used a statistical software program (Statgraphics Centurion® XVII).

The AC release at physiological pH conditions was analyzed to evaluate the release kinetics and mechanism from the MP and MP/MMT clay composite with a semi-empirical equation developed by ***Korsmeyer*** (1983) and ***Peppas*** (1985) to describe drug release from polymeric systems (Eq. (3)):

$$\frac{M_t}{M_\infty} = kt^n \quad (3)$$

Here, M_t/M_∞ is the drug fraction released at time t, k is the release rate constant and **n** is the release exponent. The value of **n** was used to characterize different release mechanisms, such that **n = 0.5** corresponds to Fickian diffusion, values of n between 0.5 and 1.0 corresponds to a non-Fickian (anomalous) transport, and **n = 1.0** corresponds to Case II transport (relaxational). Generally, this model was used to analyze the drug release from polymeric formulations when the mechanism is not well known or when more than one type of release mechanism could be involved. The examination of the goodness of fit statistics was made by determination of R-square (R^2) [35].

3. Results and discussion

3.1. Characterization of lipid-polymer hybrid microparticles (MP)

Lipid-polymer hybrid microparticles were prepared by two-step desolvation method, which separate low molecular weight chains (LMW) to achieve uniform size distribution and reproducibility. At pH 3.0 ± 0.1 GEL (IEP=4.8-5.0) protonated lysine residues and a positive charge due to amine groups (NH_3^+) prevented uncontrolled agglomeration of GEL chains. This behavior allowed the interaction with negative charged lecithin, which is a mixture of zwitterionic and anionic phospholipids [28]. The desolvating agent was used to dehydrate GEL molecules and induce conformational stretched-coil changes and precipitation of MP [29]. Finally, GA was used as a cross-linker to further harden and stabilize the MP structure to overcome its rapid dissolution in aqueous media and avoid a fast drug release at body temperature. GA is a well-known crosslinking agent for proteins, reacting easily at room temperature with the concurrent formation of aldimine linkage (-CH=N-) between free protein amino groups. In addition, it is highly soluble in aqueous solution and a good GEL crosslinking agent (generating inter/intra covalent bonds). Also, GA has been used extensively with GEL to prepare nano-carriers for insulin delivery [21], bone tissue repair scaffolds [36], nanoparticles for oral drug delivery [28,37], intravesical cancer therapy [38] and magnetic targeted drug delivery [39].

3.1.1. Entrapment efficiency (EE%)

Entrapment of hydrophobic drugs in GEL carriers could be explained considering the preferential localization of drug inside the carrier core, which is less hydrophilic than the external aqueous environment [29]. However, lipid-polymer carriers have been employed successfully for drug delivery of low-water soluble drugs and acid labile nature in biological milieu, for instance Amphotericin B [28] and Resveratrol [12], hence these carriers were selected to load hydrophobic and low-water soluble drug AC. In this work the hybrid MP, formed by lecithin and GEL, enabled the interaction of phospholipids hydrophobic region with AC, and the interaction with GEL through their hydrophilic region. Accordingly, AC can be loaded within the lipid core and stabilized by a GEL coat [28]. The EE determined for MP is 67.30% ± 2.65 (n = 3), which is higher than that of other reports with AC-PLGA nanoparticle systems (EE 34–37%) [2]. As reported recently, loaded gelatin-stearic acid hybrid nanoparticles possess lower efficiency (EE 18–58%) than that of our systems [40].

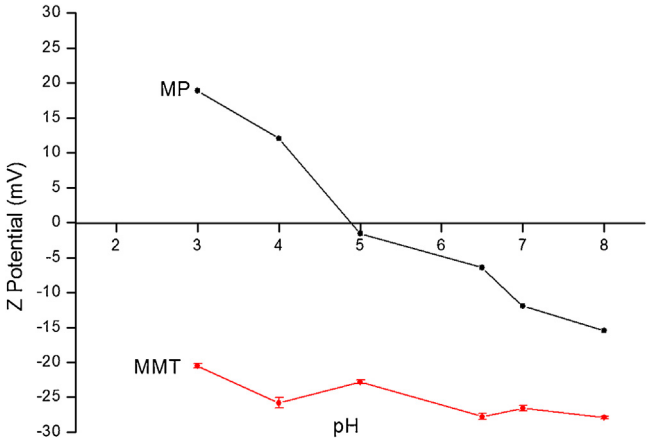

Fig. 1. pH effect on Zeta potential (ξ) for MP and MMT clay.

3.1.2. Particle size and Zeta potential (ξ)

The average size of MP was 1.42 ± 0.21 μm (n = 3) with a PDI of 0.27 ± 0.03. Unimodal size distribution was found with PDI lower than 0.5, which is an evidence of a uniform dispersion. Two-step desolvation method allowed the preparation of AC loaded hybrid MP with desirable size and PDI.

Zeta potential reflects the stability of colloidal dispersions, a high value indicates a high electric charge on the particles surface, leading to strong repellent forces between particles to prevent aggregation. A lower value of zeta potential is related to an eventually aggregation due to Van Der Waal inter-particle attractions [41]. The MP zeta potential was 22.30 ± 0.35 mV (deionized water).The MP surface charge was also evaluated in a pH range from 3.0 ± 0.1 to 8.0 ± 0.1 as shown in Fig. 1. Upon increasing the pH, a decrease in MP zeta potential was measured, confirming that the zeta potential is an inverse function of pH. This indicated that the GEL was present on the particle surface. The positive charge is primarily attributed to predominance of NH_3^+ groups, and the negative charge is due to COO^- groups. The IEP of GEL where the net charge is equal to zero was observed around pH = 4.8 ± 0.1 as reported in literature [29,32]. For the MMT clay, zeta potential in deionized water was found at −38.20 ± 0.50 mV (n = 3) in good agreement with reported data, for instance D. Zadaka et al. reported zeta potential values of Montmorillonite (MMT) from −37 mV to −42 mV [42]. In the dispersion of MMT clay (5 mg mL^{-1}) (see Fig. 1) a slight increase in zeta potential from −27.90 to −20.50 mV was observed as pH decreases. MMT has a negative charge at all pH values, but in acidic environment, an excess of protons create positive edge charges, the density of which decreases with rising pH [43].

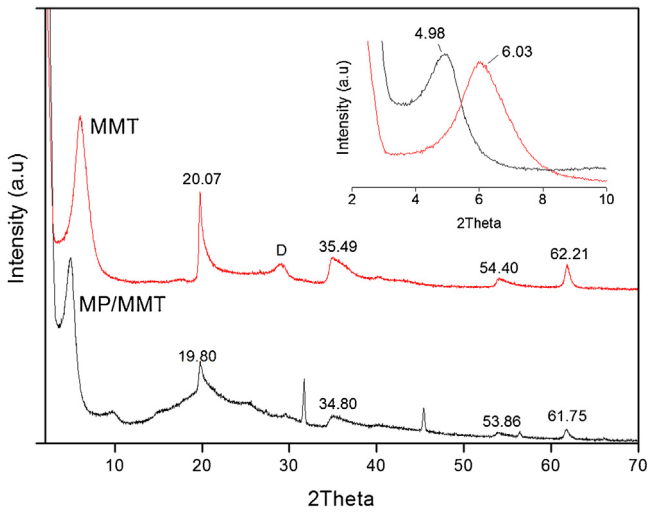

Fig. 2. XRD patterns of MMT and MP/MMT composite prepared at pH 3.0 ± 0.1.

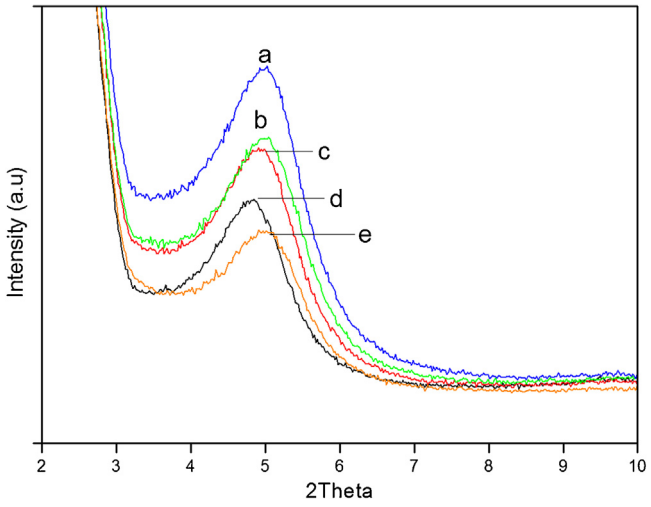

Fig. 3. pH effect on XRD patterns of MP/MMT composite: a-pH 7.0 (2θ 5.05), b- pH 6.5 (2θ 5.03), c-pH 3.0 (2θ 4.98), d-pH 1.6 (2θ 4.69) and e-pH 5.0 (2θ 5.08).

3.2. Characterization of microparticles/Montmorillonite clay composite (MP/MMT)

There are several of methods to determine CEC, but methylene blue adsorption is faster and widely used. The estimated CEC value of MMT clay raw powder was 75.77 ± 2.39 meq 100 g^{-1} (n = 3) according to the literature (70–130 meq 100 g^{-1}) [44]. The DLS particle size of MMT dispersion after magnetic stirring amounted 1.9 μm, and after sonication it was 478.7 ± 24.38 nm with PDI of 0.391 ± 0.014 (n = 3), indicating that after the sonication process the MMT was well-dispersed since the particle size was around 500 nm which is a value previously reported [41] and the surface area (S_{BET}) was 54.94 m^2 g^{-1}. The process of intercalation of polymers chains and colloidal dispersions is well known. The polymer intercalation in MMT clay in aqueous medium is driven by displacement of surface-associated water molecules. But, in our work, the intercalation was performed at pH = 3.0 ± 0.1 consisting in the adsorption of negative charged MMT (ξ −20.5 ± 0.30 mV) on the positive charged MP surface (ξ 18.87 ± 0.25 mV), and so the process was driven by a strong electrostatic attraction. The preparation of hybrid materials using electrostatic interactions of polymer and inorganic nanoparticles has been previously reported by direct addition method, which consists of mixing both components together to form aggregates of the two oppositely charged materials. After water evaporation, the dispersion re-assembled producing exfoliated/intercalated structures. However, a proportion of the layers may stack again in parallel re-forming the tactoids [45].

In the MP/MMT composite particles the zeta potential diminished (ξ 11.10 ± 0.64 mV) indicating that hybrid particles were partially covered by the MMT clay. This result corroborates the electrostatic adsorption between MMT clay and MP. In addition, an increase in size to 5.77 ± 0.60 μm (n=3) with a PDI of 0.28 ± 0.03 was observed, which is likely to be caused by the MMT adsorption to the MP leading to the new raspberry-like structure, this increase in particle size indicates the formation of a different structure from MP or MMT alone. Other authors reported similar results with different systems, for instance Xu et al. (2014) mentioned that the particle distributions are broader and the sizes are bigger in composite particles than those of the pure polymer particles, due to the presence of MMT [46].

XRD patterns allowed to investigate the pH effect on the MP/MMT composite preparation (Fig. 2). The Braggís law $\boldsymbol{n\lambda = 2dsin\theta}$, where $\boldsymbol{n}$ is a positive integer and $\boldsymbol{\lambda}$ is the incident wave wavelength was used to calculate the crystallographic space $\boldsymbol{d}$ [44].

The d_{001}, d_{003}, $d_{020\text{-}110}$, $d_{130\text{-}200}$, and d_{060} diffractions of the main MMT component were observed at 6.03, 19.80, 34.80 and 61.75 (2θ). Also, a peak from the non-clay component Dolomite (D) was observed at 29.05 (2θ) [44]. MMT reflection at 2θ = 6.03 indicated a basal spacing of 14.65 Å, whereas a major shifting to a lower diffraction angle 2θ = 4.98 with expansion of basal spacing up to 17.74 Å was observed in the MP/MMT composite. The increase in the basal spacing provided evidence of intercalation of the GEL in the interlayer space of the clay. Besides, there was a decrease in intensity in the other MMT characteristics reflections [25].

The Fig. 3 illustrates the pH effect (namely pH ± 0.1 = 1.6, 3.0, 5.0, 6.5 and 7.0) on the XRD diffraction patterns in MP/MMT composite. The interaction was highlighted by the appearance of the peak around 2θ = 4.69°–5.08° (***d*** spacing 18.85–17.74 Å) whose ***d*** increased as the pH decreased, except for pH values close to IEP. These results may be explained according to the existing interactions of MP surface with MMT clay. It is well known that GEL possesses amphoteric properties, so at pH values of 1.6 ± 0.1 and 3.0 ± 0.1 (pH<IEP), GEL has a positive surface charge due to NH_3^+ groups, interactions with MMT negative faces is promoted, as reflected by an increase in ***d*** spacing to 18.85 and 17.74 Å respectively. Moreover, at pH = 6.5 ± 0.1 and 7.0 ± 0.1 (pH>IEP) the MP have a negative surface charge due to COO^- groups coordinating with MMT laminae, but with lower interaction level which was reflected in lower increase in ***d*** spacing (17.55 and 17.51 Å). At pH>IEP the interaction between GEL and MMT occurs through the pH-dependent edges charge. Moreover, hydrogen bridge interactions between carbonyl groups in GEL and MMT hydroxyl groups also exist. However, at pH 5.0 ± 0.1 (pH ∼ IEP) the GEL ionization degree was lower, leading to the lowest increase of ***d*** spacing to 17.39 Å. Our results were in general agreement with previous reports and revealed the complex interaction between both materials[30,47,48].

The FT-IR spectra of MP, MP/MMT composite and raw materials allowed to find evidence of interactions, compatibility and crosslinking. The AC spectra is shown in Fig. 4, revealing characteristic peaks of aromatic (N—H) stretching and (C=O) stretching at 3234 cm^{-1} and 1649 cm^{-1}. In addition, peaks at 3365 cm^{-1} from (—OH) and 2972 cm^{-1} of (—CH3), 1579 cm^{-1} of (C—N) and 1432 cm^{-1} corresponding to (C—C) are observed [6]. The GEL spectra showed the characteristic absorption band for amide A (N—H) as stretching vibration at 3306 cm^{-1}, amide B at 3071 cm^{-1}, 1636 cm^{-1} of (C=O) stretching of amide I and (N—H) bend at 1534 cm^{-1} of amide II [26,49]. The lecithin spectra showed peaks

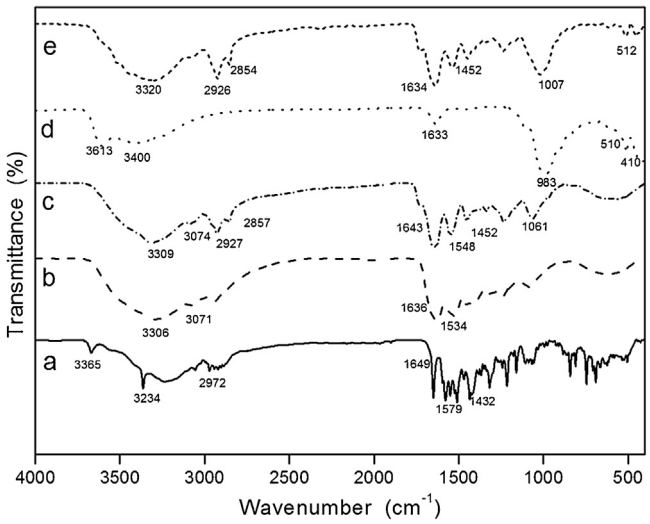

Fig. 4. FT-IR spectra of Atorvastatin (a), gelatin (b), hybrid microparticles (c), Montmorillonite clay (d), and MP/Montmorillonite composite (e).

at 1737 cm^{-1} for the vibrational signal of (C═O) and at 1227, 1060 and 824 cm^{-1} of (PO_2) [50]. In the AC loaded MP, spectra depicted the characteristics bands of amide A (3307 and 3309 cm^{-1}), amide B (3074 and 3071 cm^{-1}), amide I (1634 cm^{-1}) and amide II (1548 and 1543 cm^{-1}) indicating a major amount of GEL. In addition, the peak observed at 1452 cm^{-1} was due to aldimine (CH═N) absorption, which is a strong evidence indicating the cross-linking in MP [21]. The bands of AC were hidden by the GEL and lecithin bands. The MMT spectra depicted a broad band near to 3400 cm^{-1} due to (—OH) stretching band for interlayer water. The band at 3613 cm^{-1} is due to the (—OH) stretching in (Al—Al—OH) and (Al—Mg—OH). The characteristic peaks at 1022, 988 and 403 cm^{-1} corresponds to the (Si—O—Si) stretching band. Bands at 693 and 520 cm^{-1} are attributed to (O—Si—O) and (Al—Si—O) vibrations [44]. In the MP/MMT composite, spectra revealed characteristic bands of GEL around 3300 and 1634 cm^{-1} from amide A and B, and the characteristic signal of crosslinking aldimine at 1452 cm^{-1} corresponding to MP, in addition to MMT bands around 512 cm^{-1} indicating the composite composition.

3.3. Shape and morphology by scanning electron microscopy (SEM)

The shape and surface morphology were determined by SEM. Fig. 5**A** illustrates the spherical morphology and smooth surface, without cracks or heterogeneitie of the MP sample. The SEM image of MP/MMT composite (Fig. 5**B**) revealed MMT clay particles randomly adsorbed onto the MP surface, leading to a rough and irregular surface maintaining the spherical shape of the original MP system [26]. The composite depicted a *raspberry-like* or *armor* morphology, consisting in organic cores coated with inorganic particles [51]. This morphology was previously reported in systems such as silver/polypirrole composites attached to the surface of silica spheres [52] and polystyrene/laponite composites [53]. Despite of the existence of reports on the preparation of GEL/MMT composites for controlled drug delivery, no *raspberry-like* structures have been mentioned so far. Moreover, the addition of MMT inside GEL carriers reduces the entrapment efficiency of drugs [17,26,27]. In our system, this effect can be avoided by the localization of MMT clay on the MP surface preventing fast release and allowing the maximum EE% and drug loading capacity. However, different ratios of MP and MMT clay should be explored in future studies, to evaluate the ratio effect on morphology and drug release more thoroughly.

To evaluate the pH effect on morphology, SEM was performed at pH below the GEL IEP (pH 3.0 ± 0.1) and above IEP (pH 7.0 ± 0.1). At pH 3.0 ± 0.1, Fig. 5**C** illustrates the afore-mentioned *raspberry-like* structure due to the adsorption of negative permanent charged MMT layers on the MP surface by electrostatic attraction. While at pH 7.0 ± 0.1, Fig. 5**D** illustrates that MP preserved their smooth surface, since MP and MMT clay are negatively charged, preventing the adsorption of MMT layers on the MP surface.

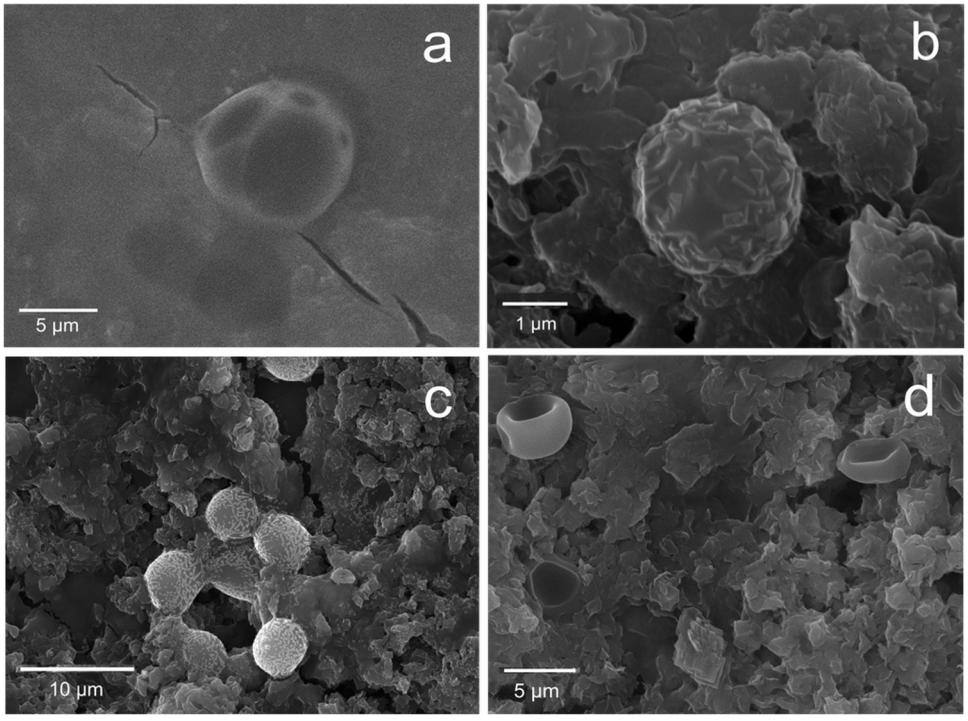

Fig. 5. SEM images of MP (a), MP/MMT composite prepared at pH 3.0 ± 0.1 (b–c), MP/MMT composite prepared at pH 7.0 ± 0.1 (d).

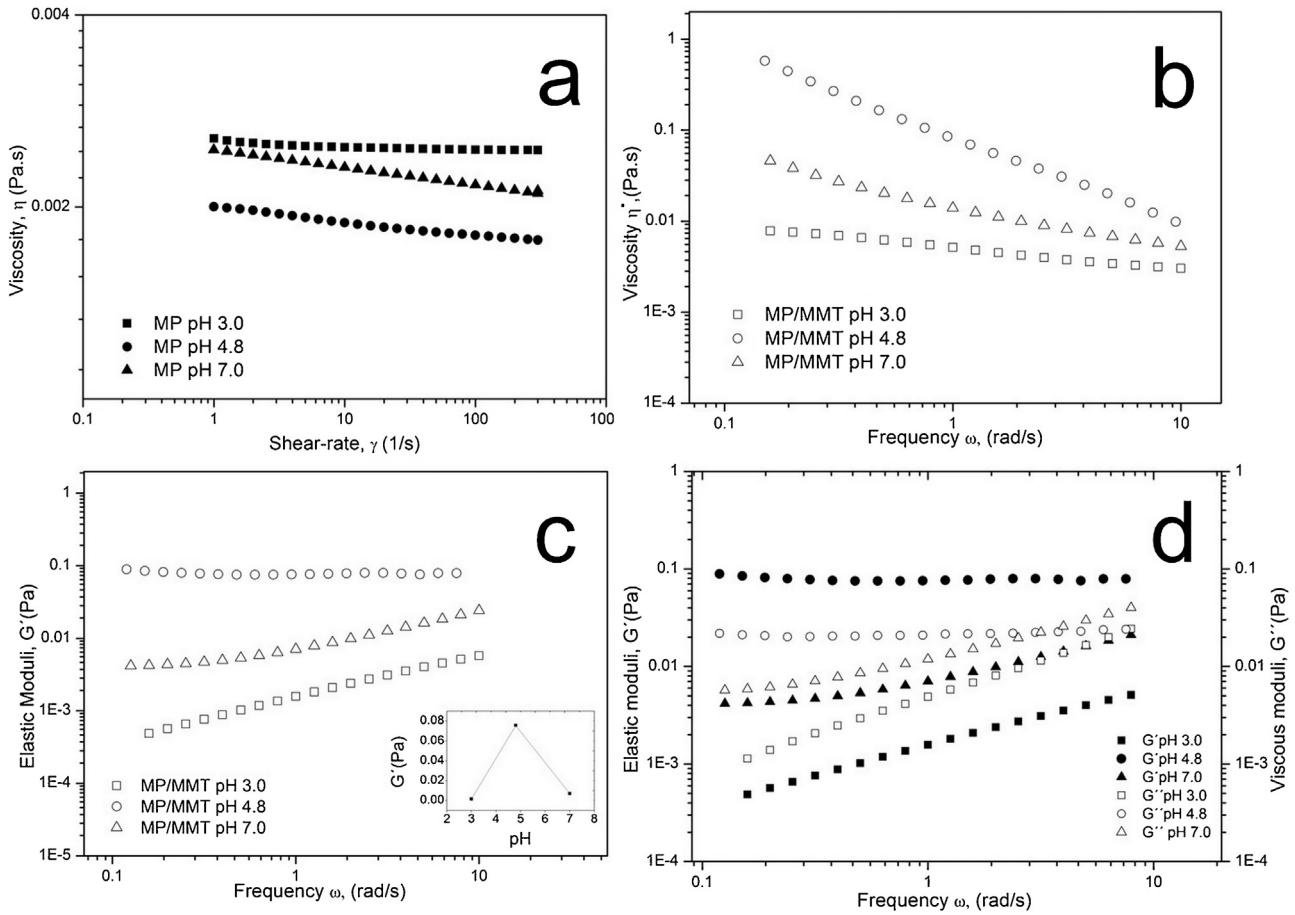

Fig. 6. pH effect (pH = 3.0 (■), 4.8 (●) and 7.0 (▲)) on the rheological behavior of MP (solid symbols) and MP/MMT composite particle-forming solutions (open symbols). MP viscosity vs shear rate (a), MP/MMT complex viscosity vs frequency (b), MP/MMT G′vs frequency (c) and MP/MMT G′G″ *vs* frequency (d).

3.4. Rheological characterization

The rheological behavior was analyzed according to the pH in the composite particle forming-solution (CFS). Under steady simple-shear the viscosity (η) depends on pH, being Newtonian in the MP system alone (Fig. 6**A**) at all pH values. Magnitudes of viscosity amounted to follows: η 3.0 ± 0.1 (pH<IEP)> η 7.0 ± 0.1 (pH > IEP)> η 4.8 ± 0.1 (pH=IEP). At pH values above and below IEP, strong positive or negative charges produced electrostatic repulsion between GEL chains, allowing relaxation and increasing water uptake, with increasing η. The Newtonian behavior stems from the feeble interaction among the spherical particles observed in SEM. However, the addition of clay induced a significant increase in the complex viscosity (η*) and a change to a non-Newtonian shear thinning behavior (n < 1) for MP/MMT system (Fig. 6**B**), as the complex viscosity decreased with increasing frequency (ω) [54]. The non-Newtonian behavior was caused by the clay which associated to form structures that were susceptible to flow-induced changes. The η* is pH-dependent, resulting from MP and MMT interactions, with a maximum η* at pH = IEP. Viscosities follow the order η* 4.8 ± 0.1 (pH = IEP) > η* 7.0 ± 0.1 (pH > IEP) > η* 3.0 ± 0.1 (pH < IEP). These results were agreement to those reported in the literature for similar GEL/MMT systems [48].

The pH-dependent edge charge of MMT allowed for different modes of associations between particles such as face-to-face (F-F), edge-to-edge (E-E) and edge-to-face (E-F). At acidic pH (below IEP), structure formation occurring due to the electrostatic attraction between negatively charged faces and positively charged edges (E-F) appeared. Hence, MMT particles associate in the so called *"house-of-cards"* structure [55], but this structure was weakened with positively charged MP. Thus, at pH 3.0 ± 0.1, the lowest η* value was corresponded to the less frequency-dependent behavior (Fig. 6**B**).

Conversely, at high pH values (above IEP), edges and faces of MMT are negatively charged. Here, structure formation was due to the long-range electrostatic repulsion (E–E and F-F). Moreover, at this pH (7.0 ± 0.1) negatively charged hybrid MP appeared, allowing a stronger "*house-of cards*" structure, with a large complex viscosity and pronounced frequency-dependent behavior (Fig. 6**B**). Interactions between MMT and MP revealed a *"solid-like"* behavior (see Fig. 6**C,** dominant viscous behavior G″ > G′ but with a frequency independent plateau) observed at low frequencies. At IEP (pH 4.8 ± 0.1), hybrid MP are neutral and do not interfere in the MMT particle association. Instead, they allowed (E-F) associations, which lead to the strongest *"house-of-cards"* structure, observed in Fig. 6**B**. This structure showed the highest η* viscosity, as reported elsewhere for similar systems [18,19].

Fig. 6**C** shows the results of the linear viscoelastic oscillatory tests. The inset depicts the elastic modulus $G'_{(\omega = 1 rad/s)}$ as function of pH. G′ attains a maximum at IEP (pH = 4.8 ± 0.1) followed by a decrease for pH values far from IEP (pH 3.0 ± 0.1 and 7.0 ± 0.1). These results support pH-dependent elasticity of the MP/MMT composite. At pH = IEP the composite presents a highly elastic structure based on a continuous network ("*house-of-cards*") which relaxes as the system moves away from IEP [18,19]. It is important to mention that at pH 3.0 ± 0.1 and 7.0 ± 0.1, the viscous character dominated along the entire range of frequencies (G″ > G′), but at pH 4.8 ± 0.1 the elastic character dominated (G′ > G″í) corresponding to a *semi-solid* behavior (see Fig. 6**D**).

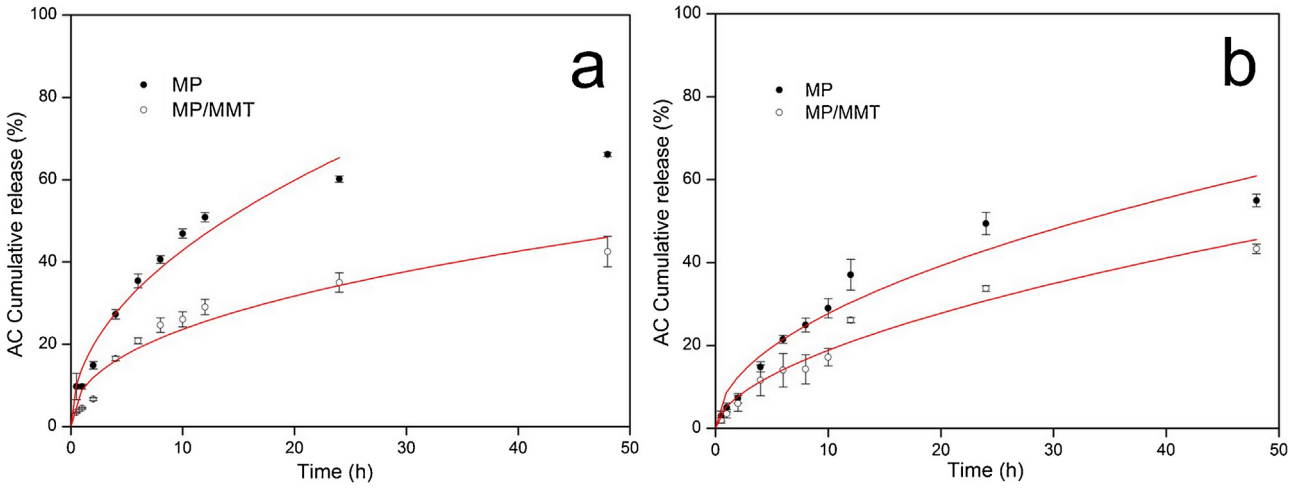

Fig. 7. *In vitro* release profile of AC from MP and MP/MMT composite in FAS state (a: hybrid microparticles (●), MP/MMT composite (○), mean ± SD, n = 3) and FED state (b: hybrid microparticles (●), MP/MMT composite (○), mean ± SD, n = 3). Symbols corresponds to experimental data; solid line corresponds to the 60% drug release fitted to Korsmeyer-Peppas model.

3.5. In vitro *drug release studies*

When formulations are administered orally, they pass through different gastrointestinal regions where they are exposed to different pH conditions. To account for such path, the *in vitro* release of AC was evaluated in various pH media that simulated the GIT environment and transit time at corporal temperature (37.0 °C ± 1 °C). *In vitro* release profile from MP and MP/MMT composite were examined during 48 h with the dialysis bag method under gastric, intestinal and colonic conditions for both FAS (Fig. 7**A**) and FED states (Fig. 7**B**). An immediate release in gastric conditions was retarded, releasing only 14.89% for FAS state (pH 1.6 ±0.1) and 5.24% with the FED state (pH 5.0 ± 0.1) within 2 h. At intestinal condition it can be seen that AC cumulative release was 40.60% for FAS (pH 6.5 ± 0.1) and 17.84% for FED (pH 5.8 ± 0.1). The release profile observed at FAS and FED mediums was delayed, after which the release was continuous and in a controlled manner during 48 h. The release profile depicted an initial rapid release period during 12 h, followed by a slower release rate up to 48 h. The biphasic pattern of drug release observed is similar to that reported elsewhere [40]. Moreover, a significant difference ($p < 0.05$) past 48 h occurred, the cumulative% AC release under FAS state (pH 7.0 ± 0.1) amounted to 66.13%, which is larger and faster than that of the FED state (pH 7.0 ± 0.1) with 54.99%.

The drug release from GEL carriers involves desorption, diffusion and biodegradation. In addition, crosslinking has been reported to have a significant impact on the drug release rate [29]. When the AC loaded MP are in contact with the release medium, solvent molecules diffuse to the GEL network followed by subsequent relaxation of GEL chains. Therefore, the AC molecules dissolve in the medium and release out through channels. The significant difference ($p < 0.05$) in the FAS and FED profile release of MP may be due to the role of pH in regulating water sorption and swelling of MP as a function of GEL-IEP. At acidic (pH<IEP i.e., 1.6 ± 0.1) or basic pH (pH > IEP i.e., 5.8 ± 0.1, 6.5 ± 0.1 and 7.0 ± 0.1) swelling increases by electrostatic repulsions, attaining the minimum value at IEP (pH ∼ IEP i.e., 5.0 ± 0.1) [26]. However, one of the most important effects of clays in polymeric systems is the dramatic improvement of barrier properties. In the MP/MMT composite, delayed releases with respect to the MP alone occurred. The presence of MMT modified the AC release through two basic mechanisms. One is the improvement of the barrier properties by the creation a tortuous path that retards the diffusion of drug molecules from MP and decreasing the solvent uptake. The other limits the swelling behavior of GEL by electrostatic attraction [14,30]. Both MP and MP/MMT composite sustained the release of AC for a long periods (48 h) even in the more extreme pH conditions. This result suggested that the MP/MMT composite allowed the maximum% of AC release in the intestinal and colonic regions where the AC can be absorbed more efficiently.

At pH = 1.6 ± 0.1 (pH<IEP) the positively-charged MP surface attracted negatively charged MMT particles, reducing swelling [48]. At pH = 5.0 ± 0.1 (pH ∼ IEP), the MP surface is neutral resulting in similar values ($p > 0.05$) of cumulative release percentage between MP and MP/MMT composite. Under these conditions, MP drives the AC release, because of poor interactions with MMT. At pH = 5.8 ± 0.1, 6.5 ± 0.1 and 7.0 ± 0.1 (pH > IEP) the MP surface is charged negatively, thus reducing the interaction with MMT, allowing the AC release.

The AC release profiles were fitted to the Korsmeyer-Peppas model with a good fit (R^2 = 0.91–0.97), and Table 1 summarizes the parameters obtained. The release rate of the composite followed different kinetics depending on the pH release medium, being controlled by interaction between GEL and MMT. A decrease in release rate (kKP) occurred with MMT. Both MP and MP/MMT composite have *n*-values corresponding to a Fickian diffusion release in

Table 1
AC cumulative release (%) and Kormeyer-Peppas parameters for MP and MP/MMT composite in FAS and FED conditions, mean ± SD, n = 3. (*Statistically significant difference ($p < 0.05$) for FAS, ** and for FED).

PARAMETER	MP FAS	MP/MMT FAS	MP FED	MP/MMT FED
SGF (n = 3) ± SD	14.89 ± 0.89*	6.67 ± 0.34*	7.26 ± 1.14	6.02 ± 1.90
SIF (n = 3) ± SD	40.60 ± 0.95*	22.26 ± 1.09*	22.54 ± 1.85**	14.10 ± 3.62**
SCF (n = 3) ± SD	66.13 ± 0.53*	42.53 ± 3.71*	54.99 ± 0.57**	43.29 ± 1.50**
kKP (n = 3) ± SD	15.75 ± 0.43	7.96 ± 0.34	7.21 ± 1.03	4.78 ± 1.74
n (n = 3) ± SD	0.41 ± 0.005	0.47 ± 0.02	0.57 ± 0.04	0.60 ± 0.12
R^2	0.9140	0.9741	0.9467	0.9483

FAS (n = 0.41 and 0.47), since for pH < IEP (1.6) and pH > IEP (6.5 and 7.0). For FED state an anomalous release (non-Fickian) (n = 0.57 and 0.60) appeared, since pH values corresponded to pH ∼ IEP (5.0) and pH > IEP (5.8 and 7.0). In this case, AC release involved a complex mechanism including Fick diffusion and erosion. The slightly increase in *n*-values for MP/MTT composite with respect to MP alone indicated the increasing restriction in drug release by MMT [56].

These results revealed that the new MP/MMT composite is a good candidate and promising drug release system for controlled intestinal-colonic drug delivery, reducing the AC release in stomach-like environment controlled by the pH of GIT.

4. Conclusions

A novel hybrid lipid-polymer MP/MMT composite with high drug entrapment efficiency (>60%) was prepared and characterized using size and zeta potential, XRD, FT-IR, SEM and rheometry. The degree of interaction between the MMT clay and MP estimated by XRD experiments revealed strong pH-dependency. SEM images depicted a new *raspberry-like* structure with adsorption of MMT on the MP surface caused by electrostatic attraction. Future work on different ratios of MP to MMT to better tune the swelling/release relationship should be considered.

A non-Newtonian behavior is observed (n < 1) in MP/MMT composite water dispersions at all pH studied. The complex viscosity (η^*) is pH-dependent, resulting from MP and MMT interactions, with a maximum η^* at pH=IEP. Additionally, at pH 3.0 ± 0.1 and 7.0 ± 0.1, the viscous character dominates along the entire frequency range ($G'' > G'$), but at pH of 4.8 ± 0.1, the elastic character dominates ($G' > G''$) corresponding to a *semi-solid* behavior. Moreover, the storage modulus (G') attains a maximum at IEP (pH=4.8 ± 0.1), whereas for pH values far from IEP (pH 3.0 ± 0.1 and 7.0 ± 0.1), lower values appeared. These results support the pH-dependent elasticity of the MP/MMT composite, and at pH=IEP the composite presents a highly elastic structure based on a continuous network ("*house-of-cards*").

Finally, the MP and MP/MMT systems revealed controlled drug release of AC during 48 h whit pH-dependent drug rate and release mechanism. This new composite is a straightforward low-cost and attractive drug delivery system intended for intestinal-colonic controlled release. Future studies will include *in vivo* controlled release experiments and pharmacokinetics evaluation of these systems.

Conflicts of interest

The authors declare that there are not any conflicts of interest regarding this work.

Acknowledgments

This research was supported by Consejo Nacional de Ciencia y Tecnología (CONACYT) [grant number 240052 and 235880].

Appendix A. Supplementary data

Supplementary data associated with this article can be found, in the online version, at https://doi.org/10.1016/j.colsurfb.2018.04.020.

References

[1] M. Anwar, M.H. Warsi, N. Mallick, S. Akhter, S. Gahoi, G.K. Jain, S. Talegaonkar, F.J. Ahmad, R.K. Khar, Enhanced bioavailability of nano-sized chitosan-atorvastatin conjugate after oral administration to rats, Eur. J. Pharm. Sci. 44 (2011) 241–249, http://dx.doi.org/10.1016/j.ejps.2011.08.001.

[2] A.K. Meena, D.V. Ratnam, G. Chandraiah, D.D. Ankola, P.R. Rao, M.N.V.R. Kumar, Oral nanoparticulate atorvastatin calcium is more efficient and safe in comparison to lipicure in treating hyperlipidemia, Lipids 43 (2008) 231–241, http://dx.doi.org/10.1007/s11745-007-3142-5.

[3] Z. Li, W. Tao, D. Zhang, C. Wu, B. Song, S. Wang, T. Wang, M. Hu, X. Liu, Y. Wang, Y. Sun, J. Sun, The studies of PLGA nanoparticles loading atorvastatin calcium for oral administration in vitro and in vivo, Asian J. Pharm. Sci. 12 (2017) 285–291, http://dx.doi.org/10.1016/j.ajps.2016.08.006.

[4] A.B. Ahmed, R. Konwar, R. Sengupta, Atorvastatin calcium loaded chitosan nanoparticles: in vitro evaluation and in vivo pharmacokinetic studies in rabbits, Braz. J. Pharm. Sci. 51 (2015) 467–477, http://dx.doi.org/10.1590/S1984-82502015000200024.

[5] N. Kumar, S. Chaurasia, R.R. Patel, G. Khan, B. Mishra, Atorvastatin calcium encapsulated eudragit nanoparticles with enhanced oral bioavailability, safety and efficacy profile, Pharm. Dev. Technol. 22 (2017) 156–167, http://dx.doi.org/10.3109/10837450.2015.1108983.

[6] N. Kumar, S. Chaurasia, R.R. Patel, G. Khan, V. Kumar, B. Mishra, Atorvastatin calcium loaded PCL nanoparticles: development, optimization, in vitro and in vivo assessments, RSC Adv. 6 (2016) 16520–16532, http://dx.doi.org/10.1039/c5ra26674b.

[7] L. Zhang, L. Zhang, Lipid–Polymer hybrid nanoparticles: synthesis, characterization and applications, Nano Life 1 (2010) 163–173, http://dx.doi.org/10.1142/S179398441000016X.

[8] L. Zhang, J.M. Chan, F.X. Gu, J.W. Rhee, A.Z. Wang, A.F. Radovic-Moreno, F. Alexis, R. Langer, O.C. Farokhzad, Self-assembled lipid-polymer hybrid nanoparticles: a robust drug delivery platform, ACS Nano 2 (2008) 1696–1702, http://dx.doi.org/10.1021/nn800275r.

[9] B. Mandal, N.K. Mittal, P. Balabathula, L.A. Thoma, G.C. Wood, Development and in vitro evaluation of core-shell type lipid-polymer hybrid nanoparticles for the delivery of erlotinib in non-small cell lung cancer, Eur. J. Pharm. Sci. 81 (2016) 162–171, http://dx.doi.org/10.1016/j.ejps.2015.10.021.

[10] K. Hadinoto, A. Sundaresan, W.S. Cheow, Lipid −polymer hybrid nanoparticles as a new generation therapeutic delivery platform: a review, Eur. J. Pharm. Biopharm. 85 (2013) 427–443, http://dx.doi.org/10.1016/j.ejpb.2013.07.002.

[11] B. Mandal, H. Bhattacharjee, N. Mittal, H. Sah, P. Balabathula, L.A. Thoma, G.C. Wood, Core-shell-type lipid-polymer hybrid nanoparticles as a drug delivery platform, Nanomedicine Nanotechnology, Biol. Med. 9 (2013) 474–491, http://dx.doi.org/10.1016/j.nano.2012.11.010.

[12] S. Kumar, P. Sangwan, V. Lather, D. Pandita, Biocompatible PLGA-oil hybrid nanoparticles for high loading and controlled delivery of resveratrol, J. Drug Deliv. Sci. Technol. 30 (2015) 54–62, http://dx.doi.org/10.1016/j.jddst.2015.09.016.

[13] S. Jayrajsinh, G. Shankar, Y.K. Agrawal, L. Bakre, Montmorillonite nanoclay as a multifaceted drug-delivery carrier: a review, J. Drug Deliv. Sci. Technol. 39 (2017) 200–209, http://dx.doi.org/10.1016/j.jddst.2017.03.023.

[14] C. Viseras, C. Aguzzi, P. Cerezo, M.C. Bedmar, Biopolymer–clay nanocomposites for controlled drug delivery, Mater. Sci. Technol. 24 (2008) 1020–1026, http://dx.doi.org/10.1179/174328408X341708.

[15] US FDA, Evaluation of the Health Aspects of Bentonite and Clay (Kaolin) as Food Ingredients, 1974.

[16] A. Gujjari, B.V. Rodriguez, J. Pescador, C. Maeder, G.W. Beall, L.K. Lewis, Factors affecting the association of single- and double-stranded RNAs with montmorillonite nanoclays, Int. J. Biol. Macromol. 109 (2018) 551–559, http://dx.doi.org/10.1016/j.ijbiomac.2017.12.124.

[17] S. Lal, M. Datta, In vitro prolonged gastric residence and sustained release of atenolol using novel clay polymer nanocomposite, Appl. Clay Sci. 114 (2015) 412–421, http://dx.doi.org/10.1016/j.clay.2015.06.017.

[18] J.D.G. Durán, M.M. Ramos-Tejada, F.J. Arroyo, F. González-Caballero, Rheological and electrokinetic properties of sodium montmorillonite suspensions, J. Colloid Interface Sci. 229 (2000) 107–117, http://dx.doi.org/10.1006/jcis.2000.6956.

[19] F. Karimi, N. Taheri Qazvini, R. Namivandi-Zangeneh, Fish gelatin/Laponite biohybrid elastic coacervates: a complexation kinetics-structure relationship study, Int. J. Biol. Macromol. 61 (2013) 102–113, http://dx.doi.org/10.1016/j.ijbiomac.2013.06.054.

[20] A.K. Bajpai, J. Choubey, Design of gelatin nanoparticles as swelling controlled delivery system for chloroquine phosphate, J. Mater. Sci. Mater. Med. 17 (2006) 345–358, http://dx.doi.org/10.1007/s10856-006-8235-9.

[21] S. Goswami, J. Bajpai, A.K. Bajpai, Designing gelatin nanocarriers as a swellable system for controlled release of insulin: an In-Vitro kinetic study, J. Macromol. Sci. Part A Pure Ans Appl. Chem. 47 (2009) 119–130, http://dx.doi.org/10.1080/10601320903458556.

[22] R. Hafidz, C. Yaakob, Chemical and functional properties of bovine and porcine skin gelatin, Int. Food Res. J. 18 (2011) 813–817.

[23] S.K. Samal, M. Dash, S. Van Vlierberghe, D.L. Kaplan, E. Chiellini, C. van Blitterswijk, L. Moroni, P. Dubruel, Cationic polymers and their therapeutic potential, Chem. Soc. Rev. 41 (2012) 7147–7194, http://dx.doi.org/10.1039/c2cs35094g.

[24] M. Santoro, A.M. Tatara, A.G. Mikos, Gelatin carriers for drug and cell delivery in tissue engineering, J. Control. Release 190 (2014) 210–218, http://dx.doi.org/10.1016/j.jconrel.2014.04.014.

[25] B.D. Kevadiya, S. Rajkumar, H.C. Bajaj, S.S. Chettiar, K. Gosai, H. Brahmbhatt, A.S. Bhatt, Y.K. Barvaliya, G.S. Dave, R.K. Kothari, Biodegradable gelatin-ciprofloxacin-montmorillonite composite hydrogels for controlled drug release and wound dressing application, Colloids Surf. B Biointerfaces 122 (2014) 175–183, http://dx.doi.org/10.1016/j.colsurfb.2014.06.051.

[26] M. Sarmah, N. Banik, A. Hussain, A. Ramteke, H.K. Sharma, T.K. Maji, Study on crosslinked gelatin-montmorillonite nanoparticles for controlled drug delivery applications, J. Mater. Sci. 50 (2015) 7303–7313, http://dx.doi.org/10.1007/s10853-015-9287-3.
[27] S. Jain, M. Datta, Montmorillonite-PLGA nanocomposites as an oral extended drug delivery vehicle for venlafaxine hydrochloride, Appl. Clay Sci. 99 (2014) 42–47, http://dx.doi.org/10.1016/j.clay.2014.06.006.
[28] S. Jain, P.U. Valvi, N.K. Swarnakar, K. Thanki, Gelatin coated hybrid lipid nanoparticles for oral delivery of amphotericin B, Mol. Pharm. 9 (2012) 2542–2553, http://dx.doi.org/10.1021/mp300320d.
[29] A.O. Elzoghby, Gelatin-based nanoparticles as drug and gene delivery systems: reviewing three decades of research, J. Control. Release 172 (2013) 1075–1091, http://dx.doi.org/10.1016/j.jconrel.2013.09.019.
[30] J.P. Zheng, P. Li, Y.L. Ma, K. De Yao, Gelatin/montmorillonite hybrid nanocomposite. I. Preparation and properties, J. Appl. Polym. Sci. 86 (2002) 1189–1194.
[31] American Society for testing materials, Standard Test Method for Methylene Blue Index of Clay C837-09, 2012.
[32] S. Azarmi, Y. Huang, H. Chen, S. McQuarrie, D. Abrams, W. Roa, W.H. Finlay, G.G. Miller, R. Löbenberg, Optimization of a two-step desolvation method for preparing gelatin nanoparticles and cell uptake studies in 143 B osteosarcoma cancer cells, J. Pharm. Pharm. Sci. 9 (2006) 124–132.
[33] L. Medina-Torres, E.E. GarcÍa-Cruz, F. Calderas, R.F. González Laredo, G. Sánchez-Olivares, J.A. Gallegos-Infante, N.E. Rocha-Guzmán, J. RodrÍguez-RamÍrez, Microencapsulation by spray drying of gallic acid with nopal mucilage (Opuntia ficus indica), LWT – Food Sci. Technol. 50 (2013) 642–650, http://dx.doi.org/10.1016/j.lwt.2012.07.038.
[34] M.R.C. Marques, R. Loebenberg, M. Almukainzi, Simulated biological fluids with possible application in dissolution testing, Dissolution Technol. 18 (2011) 15–28.
[35] P. Costa, Modeling and comparison of dissolution profiles, Eur. J. Pharm. Sci. 13 (2001) 123–133.
[36] M. Kazemzadeh, Fabrication of porous hydroxyapatite-gelatin composite scaffolds for bone tissue engineering, Iran. Biomed. J. 10 (2006) 215–223.
[37] M.H. El-Shabouri, Positively charged nanoparticles for improving the oral bioavailability of cyclosporin-A, Int. J. Pharm. 249 (2002) 101–108.
[38] Z. Lu, T. Yeh, M. Tsai, J.L. Au, M.G. Wientjes, Paclitaxel-Loaded gelatin nanoparticles for intravesical bladder cancer therapy, Clin. Cancer Res. 10 (2004) 7677–7684.
[39] B. Gaihre, M.S. Khil, D.R. Lee, H.Y. Kim, Gelatin-coated magnetic iron oxide nanoparticles as carrier system: drug loading and in vitro drug release study, Int. J. Pharm. 365 (2009) 180–189, http://dx.doi.org/10.1016/j.ijpharm.2008.08.020.
[40] D. Shilpi, V. Kushwah, A.K. Agrawal, S. Jain, Improved stability and enhanced oral bioavailability of atorvastatin loaded stearic acid modified gelatin nanoparticles, Pharm. Res. 34 (2017) 1505–1516, http://dx.doi.org/10.1007/s11095-017-2173-8.
[41] C.H.C. Flaker, R.V. Lourenço, Bittante A.M.Q.B, P.J.A. Sobral, Gelatin-based nanocomposite films: a study on montmorillonite dispersion methods and concentration, J. Food Eng. 167 (2015) 65–70, http://dx.doi.org/10.1016/j.jfoodeng.2014.11.009.
[42] D. Zadaka, A. Radian, Y.G. Mishael, Applying zeta potential measurements to characterize the adsorption on montmorillonite of organic cations as monomers, micelles, or polymers, J. Colloid Interface Sci. 352 (2010) 171–177, http://dx.doi.org/10.1016/j.jcis.2010.08.010.
[43] E. Tombácz, M. Szekeres, Colloidal behavior of aqueous montmorillonite suspensions: the specific role of pH in the presence of indifferent electrolytes, Appl. Clay Sci. 27 (2004) 75–94, http://dx.doi.org/10.1016/j.clay.2004.01.001.
[44] B. Caglar, B. Afsin, A. Tabak, E. Eren, Characterization of the cation-exchanged bentonites by XRPD, ATR, DTA/TG analyses and BET measurement, Chem. Eng. J. 149 (2009) 242–248, http://dx.doi.org/10.1016/j.cej.2008.10.028.
[45] M.A. Hood, M. Mari, R. Muñoz-Espí, Synthetic strategies in the preparation of polymer/inorganic hybrid nanoparticles, Materials (Basel) 7 (2014) 4057–4087, http://dx.doi.org/10.3390/ma7054057.
[46] G.Z. Xu Jingshui, Ke Yangchuan, Qian Zhou, Xianglong Hu, Zijuan Tan, Liyan Yang, Youzhi Song, Yangyang Zhao, Preparation, Structure, and properties of Poly(vinyl acetate-co-methyl methacrylate) Nanocomposite Microspheres with exfoliated Montmorillonite Through using two-stage in situ suspension polymerization, Polym. Compos. 35 (2014) 1106–1116, http://dx.doi.org/10.1002/pc.22758.
[47] J.F. Martucci, A. Vázquez, R.A. Ruseckaite, Nanocomposites based on gelatin and montmorillonite: morphological and thermal studies, J. Therm. Anal. Calorim. 89 (2007) 117–122, http://dx.doi.org/10.1007/s10973-006-7454-0.
[48] P. Li, J.P. Zheng, Y.L. Ma, K. De Yao, Gelatin/montmorillonite hybrid nanocomposite. II. swelling behavior, J. Appl. Polym. Sci. 88 (2003) 322–326.
[49] J.G. Borges, A.G. Silva, C.M. Cervi-Bitencourt, F.M. Vanin, R.A. Carvalho, Lecithin, gelatin and hydrolyzed collagen orally disintegrating films: functional properties, Int. J. Biol. Macromol. 86 (2016) 907–916, http://dx.doi.org/10.1016/j.ijbiomac.2016.01.089.
[50] J.M. Nzai, A. Proctor, Determination of phospholipids in vegetable oil by fourier transform infrared spectroscopy, J. Am. Oil Chem. Soc. 75 (1998) 1281–1289.
[51] M. Agrawal, S. Gupta, M. Stamm, Recent developments in fabrication and applications of colloid based composite particles, J. Mater. Chem. 21 (2011) 615–627, http://dx.doi.org/10.1039/c0jm02631j.
[52] T. Yao, C. Wang, J. Wu, Q. Lin, H. Lv, K. Zhang, K. Yu, B. Yang, Preparation of raspberry-like polypyrrole composites with applications in catalysis, J. Colloid Interface Sci. 338 (2009) 573–577, http://dx.doi.org/10.1016/j.jcis.2009.05.001.
[53] Y.J. Kim, Y.D. Liu, H.J. Choi, S.J. Park, Facile fabrication of Pickering emulsion polymerized polystyrene/laponite composite nanoparticles and their electrorheology, J. Colloid Interface Sci. 394 (2013) 108–114, http://dx.doi.org/10.1016/j.jcis.2012.12.040.
[54] M.F. Coronado-Jorge, C.H. Caicedo Flaker, S.F. Nassar, I.C.F. Moraes, A.M.Q.B. Bittante, P.J. Do Amaral Sobral, Viscoelastic and rheological properties of nanocomposite-forming solutions based on gelatin and montmorillonite, J. Food Eng. 120 (2014) 81–87, http://dx.doi.org/10.1016/j.jfoodeng.2013.07.007.
[55] E. Günister, S. Işçi, N. Öztekin, F.B. Erim, Ece Ö.I, N. Güngör, Effect of cationic surfactant adsorption on the rheological and surface properties of bentonite dispersions, J. Colloid Interface Sci. 303 (2006) 137–141, http://dx.doi.org/10.1016/j.jcis.2006.07.021.
[56] R.A. Bini, M.F. Silva, L.C. Varanda, M.A. da Silva, C.A. Dreiss, Soft nanocomposites of gelatin and poly(3-hydroxybutyrate) nanoparticles for dual drug release, Colloids Surf. B Biointerfaces 157 (2017) 191–198, http://dx.doi.org/10.1016/j.colsurfb.2017.05.051.